BIOCHEMISTRY
including biophysical chemistry & molecular biology

Article

pubs.acs.org/biochemistry

Evolutionarily Distinct Versions of the Multidomain Enzyme α-Isopropylmalate Synthase Share Discrete Mechanisms of V-Type Allosteric Regulation

Garima Kumar and Patrick A. Frantom*

Department of Chemistry, The University of Alabama, Tuscaloosa, Alabama 35487, United States

Supporting Information

ABSTRACT: Understanding the evolution of allostery in multidomain enzymes remains an important step in improving our ability to identify and exploit structure−function relationships in allosteric mechanisms. A recent protein similarity network for the DRE-TIM metallolyase superfamily indicated there are two evolutionarily distinct forms of the enzyme α-isopropylmalate synthase (IPMS) sharing approximately 20% sequence identity. IPMS from *Mycobacterium tuberculosis* has been extensively characterized with respect to catalysis and the mechanism of feedback regulation by L-leucine. Here, IPMS from *Methanococcus jannaschii* (MjIPMS) is used as a representative of the second form of the enzyme, and its catalytic and regulatory mechanism is compared with that of MtIPMS to identify any functional differences between the two forms. MjIPMS exhibits kinetic parameters similar to those of other reported IPMS enzymes and is partially inhibited by L-leucine in a V-type manner. Identical values of $^{D_2O}k_{cat}$ (3.1) were determined in the presence and absence of L-leucine, indicating the hydrolytic step is rate-determining in the absence of L-leucine and remains so in the inhibited form of the enzyme. This mechanism is identical to the mechanism identified for MtIPMS ($^{D_2O}k_{cat}$ = 3.3 ± 0.3 in the presence of L-leucine) despite product release being rate-determining in the uninhibited MtIPMS enzyme. The identification of identical regulatory mechanisms in enzymes with low sequence identity raises important evolutionary questions concerning the acquisition and divergence of multidomain allosteric enzymes and highlights the need for caution when comparing regulatory mechanisms for homologous enzymes.

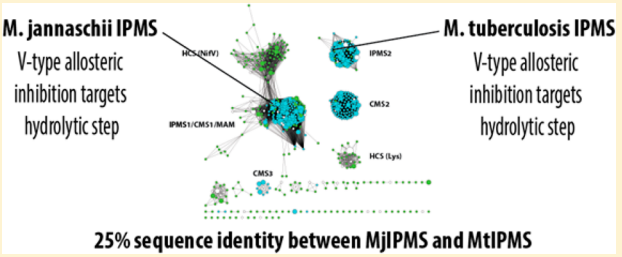

Evolution of enzyme function remains a topic of intense study in the field of biochemistry as it simultaneously addresses a fundamental biochemical problem and has potential to impact strategies used in the design enzymes with novel catalytic functions.[1] Identifying mechanisms of evolution also aids in the tremendous task of creating more robust methods for functional annotation of genome data.[2] One approach for studying enzyme evolution is the use of "genomic enzymology".[3] Through the integration of bioinformatics, structural, and kinetic studies, genomic enzymology has been used to investigate functionally diverse enzyme superfamilies and establish mechanisms of functional evolution.[4−8] Recently, this approach was applied to the DRE-TIM metallolyase superfamily.[9] Members of the DRE-TIM metallolyase superfamily catalyze a diverse set of reactions involving the making and breaking of C−C bonds. Enzymes in this superfamily use a TIM-barrel catalytic domain, a divalent metal, and conserved active site architecture, including a signature three-amino acid D-R-E motif, to stabilize a common enolate intermediate. A protein similarity network indicated four main functional subgroups associated with the superfamily: Claisen condensation-like, aldolase-like, carboxylase-like, and lyase-like.

Members of the Claisen condensation-like (CC-like) subgroup include isopropylmalate synthase (IPMS), citramalate synthase (CMS), and homocitrate synthase (HCS). These three enzymes catalyze the first step in the biosynthesis of L-leucine, L-isoleucine (pyruvate-dependent pathway), and L-lysine (α-aminoadipate pathway). In addition to the shared DRE-TIM metallolyase catalytic domain (Pfam entry PF00682), IPMS and CMS have an additional conserved C-terminal regulatory domain called the LeuA dimer regulatory domain (Pfam entry PF08502) (Figure 1A).[10,11] HCS enzymes lack this regulatory domain and are regulated through a competitive mechanism.[12] Analysis of the representative protein similarity network for the CC-like subgroup indicates there are four distinct sequence motifs defining the boundary of interaction between the two domains (four clusters of cyan nodes in Figure 1B).[9] Additionally, all three activities can be found in multiple clusters, suggesting there are differentially conserved versions of enzymes with the same function. For example, the IPMS1/CMS1/MAM and IPMS2 clusters both contain sequences encoding IPMS enzymes. This raises the question of how similar functionalities and folds arise from differentially conserved sequences. Several mechanisms have been proposed to explain similar findings in the enolase

Received: June 6, 2014
Revised: July 2, 2014
Published: July 3, 2014

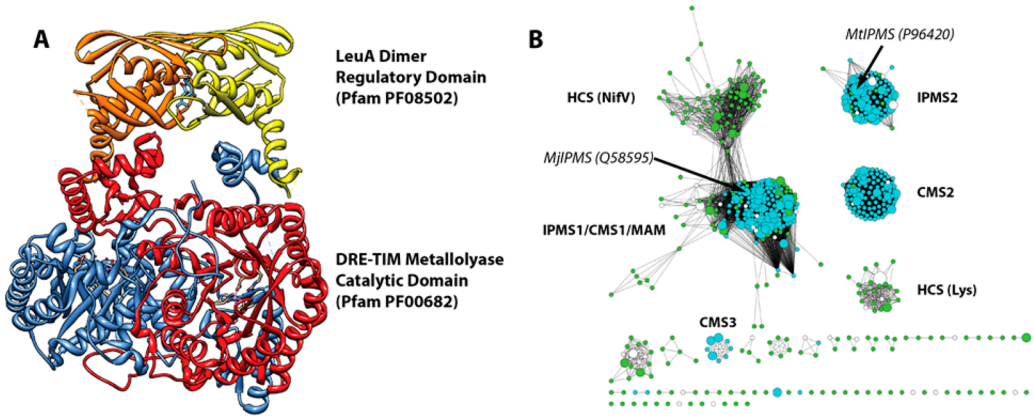

Figure 1. (A) Structure of conserved domains in IPMS enzymes. A cartoon representation of MtIPMS (Protein Data Bank entry 3fig)[10] is shown. Individual monomers are colored blue and yellow, and red and orange. Residues in the active site and L-leucine are rendered as sticks. (B) Representative network for the Claisen condensation-like subgroup of the DRE-TIM metallolyase superfamily.[9] Edges are drawn if the similarity between a pair of nodes is better than an *E* value threshold cutoff of 10^{-80}. Predicted functionalities of each cluster are indicated in bold and based on Swiss-prot curated annotations. The locations of nodes containing the sequences for MjIPMS and MtIPMS are labeled in italics. Nodes colored cyan are predicted to contain both the DRE-TIM metallolyase superfamily catalytic domain (Pfam entry: PF00682) and the LeuA dimer regulatory domain (Pfam entry: PF08502). Nodes colored green are predicted to contain only the catalytic domain. Nodes colored white are not annotated with respect to domain architecture.

Scheme 1

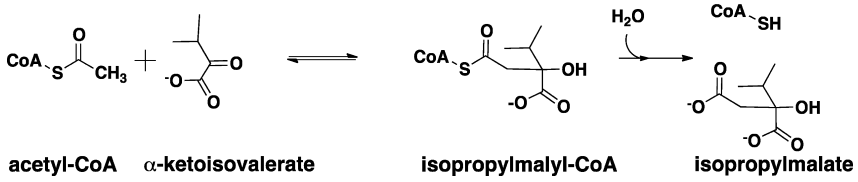

superfamily, including divergent evolution for *o*-succinylbenzoate synthases[13] and "pseudoconvergent" evolution in the cases of *N*-succinyl amino acid racemase[14] and muconate lactonizing enzyme.[15] However, the additional need for a coordinated regulatory mechanism with each distinct sequence, as required by IPMS and CMS in the CC-like subgroup, has not been investigated. This report focuses on the two clusters predicted to contain IPMS activity: the IPMS1/CMS1/MAM cluster and the IPMS2 cluster. The average level of sequence identity between representative sequences in the two clusters is <20%, while representative sequences within each cluster are on average ∼50% identical.

IPMS catalyzes the first step in the biosynthesis of L-leucine in organisms from all three domains of life. The overall enzymatic reaction is shown in Scheme 1. The first step involves condensation of acetyl-coenzyme A (AcCoA) with α-ketoisovalerate (KIV) to form an isopropylmalyl-CoA intermediate. The second step is the base-catalyzed hydrolysis of the intermediate to generate the two products, CoA and α-isopropylmalate. IPMS is subject to allosteric feedback regulation by binding of L-leucine to the LeuA dimer domain.[16] This domain is found only in connection with IPMS and CMS enzymes and responds specifically to L-leucine and L-isoleucine, respectively. Mechanisms of allosteric regulation in both IPMS and CMS are well-documented and indicate the LeuA dimer regulatory domain is capable of exhibiting both V-type (inhibition occurs by a decrease in the value of k_{cat}) and K-type (inhibition occurs by an increase in the value of K_M) allosteric mechanisms, although structure−function relationships that govern this difference are not understood.[16] In general, the quaternary structure of characterized IPMS enzymes is not affected by addition of the amino acid inhibitor, ruling out one common mechanism of allostery.

IPMS from *Mycobacterium tuberculosis* (MtIPMS) has received the most attention because of its role as a possible drug target. MtIPMS is subject to V-type inhibition by L-leucine, with inhibition exhibited in a slow-onset mechanism.[17] Results from solution-phase backbone amide hydrogen−deuterium exchange indicated that global changes are seen in the LeuA dimer domain when L-leucine binds and smaller, local changes are seen in the active site of the catalytic domain.[18] Recently, rapid reaction kinetics and kinetic isotope effects were used to identify a discrete mechanism of L-leucine inhibition in MtIPMS in which L-leucine binding perturbs the catalytic machinery associated with the hydrolytic step in the chemical mechanism (Scheme 1).[19] With a detailed description of the allosteric mechanism for MtIPMS in hand, interest turns to the conservation of allosteric mechanisms used by the distinct sequence motifs represented in the CC-like subgroup. IPMS from *Methanococcus jannaschii* (MjIPMS) was selected as a representative sequence from the IPMS1 cluster to probe the conservation of allosteric mechanism used by the LeuA dimer regulatory domain. Results are compared with those obtained with MtIPMS, which belongs to the IPMS2 cluster. Additionally, protein similarity networks were constructed to address mechanisms of co-evolution between catalytic and regulatory domains in the CC-like subgroup.

MATERIALS AND METHODS

Materials. The plasmid containing the MjIPMS gene *leuA Mj1195* was acquired from ATCC (Manassas, VA).[20] Primers for amplification of *leuA Mj1195* were obtained from Eurofins

dx.doi.org/10.1021/bi500702u | *Biochemistry* 2014, 53, 4847−4856

Genomics (Huntsville, AL). Acetyl-CoA and ketoisovalerate were purchased from Sigma-Aldrich. 4,4′-Dithiodipyridine (DTP) was purchased from Acros Organics. All other reagents and buffers were obtained from VWR and were of the highest quality available. The HisTrap HP column was obtained from GE Healthcare. Competent cells [BL21(DE3)pLysS and XL-10 Gold] were purchased from Invitrogen.

Amplification and Overexpression of MjIPMS. *leuA Mj1195* was amplified via polymerase chain reaction (PCR) from ATCC plasmid AMJHH70 (pUC18 vector) using the following primers: 5′-*GCTAG*CATAATTTATAGGGAAGAG-AATGAAATTAT-3′ (*Nhe*I site italicized) and 5′-*CTCGAG*T-CATTTTTCTCTTTTTGCCAAG-3′ (*Xho*I site italicized). The PCR product was digested using restriction endonucleases, ligated into the pET28 vector, and transformed into XL-10 Gold competent cells. Overnight cultures were grown from single colonies, and the plasmid was re-isolated and sent for sequencing to confirm the genetic integrity of the gene. Positive clones were then transformed in BL21(DE3)pLysS *Escherichia coli* cells. The plasmid-containing BL21(DE3)pLysS *E. coli* cells were grown in LB medium at 37 °C until the OD_{600} reached 0.4, and then the temperature was reduced to 18 °C. At an OD_{600} of 0.8, the culture was induced with 1 mM isopropyl β-D-1-thiogalactopyranoside (IPTG) and allowed to incubate while being shaken (250 rpm) for 12−16 h at 18 °C. The cells were harvested by centrifugation at 7000*g* for 10 min at 4 °C.

Protein Purification. Frozen cell pellets were resuspended in lysis buffer [20 mM potassium phosphate (pH 7.4), 0.5 M potassium chloride, 20 mM imidazole, and 0.1% Triton], lysozyme (0.25 mg/mL), 1 mM phenylmethanesulfonyl fluoride (PMSF), deoxyribonuclease (10 μg/mL), and magnesium chloride. Cells were lysed by sonication, and the supernatant was collected by centrifugation at 34540*g* for 30 min at 4 °C. The supernatant was heat treated via incubation in a water bath at 50 °C for 10 min followed by centrifugation 34540*g* for 10 min at 4 °C. The target protein was purified from the heat-treated supernatant using a Ni^{2+} HisTrap column (5 mL) over a linear gradient with elution buffer [20 mM potassium phosphate (pH 7.4), 0.5 M potassium chloride, and 1 M imidazole]. Protein purity was checked by sodium dodecyl sulfate−polyacrylamide gel electrophoresis. Fractions containing MjIPMS were pooled and dialyzed against 20 mM potassium phosphate (pH 7.4) and 200 mM potassium chloride. The protein was concentrated by ultrafiltration to an approximate concentration of 100 μM, as determined by the calculated extinction coefficient (ε_{280} = 21110 M^{-1} cm^{-1}). The concentrated protein was stored in 20% glycerol at −20 °C.

Steady State Assays. Initial velocities were determined by detecting the formation of CoA by DTP at 324 nm (ε = 19.8 mM^{-1} cm^{-1}). The standard conditions for a typical reaction mixture were 100 mM triethanolamine (TEA) (pH 7.8), 50 mM potassium chloride, 100 μM DTP, and a saturating concentration of the nonvaried substrate (keto-isovalerate or acetyl-CoA) in a 1 mL reaction mixture at 37 °C. Reactions were initiated by the addition of 20−30 nmol of enzyme. The diluted enzyme used for the assay was kept at room temperature. The assay conditions used to determine the mechanism of feedback inhibition by L-leucine were 100 mM TEA (pH 7.8), 50 mM potassium chloride, 100 μM DTP, 500 μM substrates, and varied leucine concentrations.

The pH dependence of k_{cat} and k_{cat}/K_M for KIV and AcCoA was determined at saturating concentrations of the nonvaried substrate in the presence of 100 mM buffers. The following buffers were used: 2-(*N*-morpholino)ethanesulfonic acid (MES) (pH 5.5−6.9), *N*-(2-hydroxyethyl)piperazine-*N*′-2-ethanesulfonic acid (HEPES) (pH 6.9−8.3), and *N*-tris-(hydroxymethyl)methyl-2-aminopropanesulfonic acid (TAPS) (pH 8.3−9.4).

Solvent Kinetic Isotope Effects. Solvent kinetic isotope effects on k_{cat} were determined by performing the assay in 99% deuterium oxide in the presence of saturating concentrations of the nonvaried substrate. All the components of the assay were made in D_2O except the diluted enzyme. To account for the effect of the viscosity of D_2O on the kinetic parameters of the enzyme, and initial velocity studies were performed in the presence of 10% glycerol. The proton inventory on k_{cat} was performed by varying the atom fraction of the deuterium oxide from 0 to 0.8 in increments of 0.2, in triplicate in the presence of saturating concentrations of substrates.

Assay conditions for determining the solvent kinetic isotope effects were 100 mM TAPS (pL 8.2), 50 mM KCl, 50 μM DTP, 20 μM L-leucine, 1000 μM KIV, and varied AcCoA concentrations.

Primary Deuterium Kinetic Isotope Effects. The standard assay conditions for determining the primary kinetic isotope effect were 100 mM TEA (pH 7.8), 50 mM KCl, 50 μM DTP, 1000 μM KIV, and varied [$^2H_3$]methyl-AcCoA concentrations. Deuterated AcCoA was synthesized as previously described[21] and determined to be 97% pure by ^1H nuclear magnetic resonance (NMR) spectroscopy. Assays for determining primary isotope effects in the presence of an inhibitor were performed under standard conditions in the presence of saturating L-leucine concentrations.

Size-Exclusion Chromatography. The quaternary structure of the enzyme was determined using size-exclusion chromatography. A GL Superdex 200 10/300 column was equilibrated with 20 mM potassium phosphate (pH 7.4) and 200 mM KCl. A molecular weight standard kit (Bio-Rad) was used to calibrate the column. To determine the effect of L-leucine on the quaternary structure of the enzyme, the experiment was repeated with the addition of 50 μM L-leucine to the running buffer. MjIPMS was incubated with 50 μM L-leucine for 20 min prior to injection on the column. The data were analyzed by plotting the log of the molecular weight of each standard protein versus the calculated K_{av} value.

Data Analyses. Kinetic parameters were determined by fitting the initial velocities to the Michaelis−Menten equation (eq 1) using Kaleidagraph (Synergy Software)

$$\frac{v}{E_t} = \frac{k_{cat}[S]}{K_m + [S]} \quad (1)$$

where [S] is the concentration of the substrate being varied, K_M is the Michaelis−Menten constant, and k_{cat} is the maximal velocity.

The effect of changes in pH on the catalytic parameters was determined by fits of the data to one of the equations describing either two residues contributing to a single acidic pK_a value (eq 2), a bell-shaped profile with two residues contributing to the acidic limb and one residue contributing to the basic limb (eq 3), or a bell-shaped profile with two residues contributing to both the acidic and basic limbs (eq 4).

dx.doi.org/10.1021/bi500702u | *Biochemistry* 2014, 53, 4847−4856

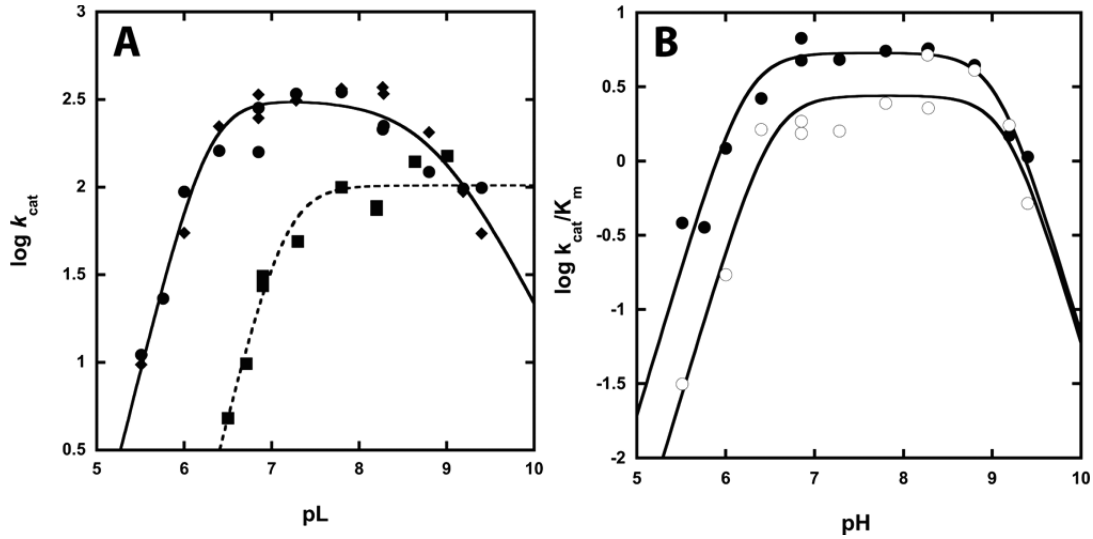

Figure 2. Effect of pH on kinetic parameters. Experimental conditions are as described in Materials and Methods. (A) Effect of pH (● and ◆) and pD (■) on k_{cat} values. Values were determined by varying either KIV (◆) or AcCoA (● and ■) at saturating concentrations of the other substrate. The solid line is a fit of the data to eq 3, and the dashed line is a fit of the data to eq 2. (B) Effect of pH on the k_{cat}/K_M values of AcCoA (●) and KIV (○). Solid lines are fits of the data to eq 4.

$$\log(x) = \log\left[\frac{(x)_{max}}{1 + \left(\frac{10^{pK_a}}{10^{pH}}\right)^2}\right] \quad (2)$$

$$\log(x) = \log\left[\frac{(x)_{max}}{1 + \left(\frac{10^{pK_a}}{10^{pH}}\right)^2 + \left(\frac{10^{pH}}{10^{pK_b}}\right)}\right] \quad (3)$$

$$\log(x) = \log\left[\frac{(x)_{max}}{1 + \left(\frac{10^{pH}}{10^{pK_b}}\right)^2 + \left(\frac{10^{pK_a}}{10^{pH}}\right)^2}\right] \quad (4)$$

where x is either k_{cat} or k_{cat}/K_M, pH is the pH value of the assay, pK_a is the pK associated with the acidic limb, and pK_b is the pK associated with the basic limb.

Primary kinetic isotope effect and solvent kinetic isotope effects in the presence of L-leucine were determined by the direct comparison method. Initial velocity data were globally fit (Grafit, Erithacus Software) to eq 5, which describes a kinetic isotope effect expressed on the k_{cat} parameter, or eq 6, which describes kinetic isotope effects on both k_{cat} and k_{cat}/K_M.

$$\frac{\nu}{E_t} = \frac{k_{cat}[S]}{K_m + [S](1 + FE_v)} \quad (5)$$

$$\frac{\nu}{E_t} = \frac{k_{cat}[S]}{K_M(1 + FE_{k_{cat}/K_m}) + [S](1 + FE_v)} \quad (6)$$

where ν is the initial velocity, E_t is the total enzyme concentration, k_{cat} is the maximal velocity, [S] is the concentration of the varied substrate (AcCoA), F is the fraction of isotope (0 for nonlabeled and 1 for fully labeled), and E_v and E_{k_{cat}/K_m} are the isotope effect on $k_{cat} - 1$ and $k_{cat}/K_M - 1$, respectively.

The proton inventory data were fit to eq 7

$$(k_{cat})_n/(k_{cat})_0 = 1 - n + n\theta \quad (7)$$

where n is the fraction of D_2O, $(k_{cat})_n$ is the value of k_{cat} at n fraction, $(k_{cat})_0$ is the value of k_{cat} in H_2O, θ is the fractionation factor.[22]

Inhibition parameters for L-leucine were determined by a fit of the data to eq 8 using Kaleidagraph

$$v_i = \frac{k_{cat}(K_i + \beta[I])}{K_i + [I]} \quad (8)$$

where [I] is the inhibitor concentration, V is the maximal velocity of the enzyme in the absence of inhibitor, v_i is the velocity in the presence of varied inhibitor concentrations, K_i is the inhibition constant of the inhibitor, and β is residual activity at saturating inhibitor concentrations.[23]

Construction of a Representative Protein Similarity Network for the DRE-TIM Catalytic Domain and LeuA Dimer Regulatory Domain of the CC-like Subgroup. Representative nodes from the Claisen condensation-like (CC-like) subgroup[9] of the DRE-TIM metallolyase superfamily predicted to contain both the DRE-TIM metallolyase catalytic domain and LeuA dimer regulatory domain were used to generate a new sequence data set (291 representative sequences). The sequences were aligned using MAFFT version 7.[24] Portions of the aligned sequences corresponding to the HMM logo for the LeuA dimer regulatory domain Pfam entry[25] were excised from the alignment and saved as a separate sequence data set. All gaps introduced in both alignments were removed to generate nonaligned sequence data sets. Sequences in both data sets were then used in an all versus all BLAST[26] search to define edges between nodes based on a matrix of E values. A Cytoscape-readable file was created in Excel to produce networks that could be explored interactively using Cytoscape version 3.1.[27] Additional information associated with each node (cluster membership) or edge (alignment length or percent sequence identity) was imported into the Cytoscape file.

dx.doi.org/10.1021/bi500702u | *Biochemistry* 2014, 53, 4847−4856

RESULTS

Assay Optimization and Steady State Kinetic Parameters. Prior to a full kinetic analysis, optimal conditions for MjIPMS activity were identified with respect to the requirement for exogenous monovalent and divalent cations (Figure S1, Supporting Information). As isolated, MjIPMS was active in the absence of exogenous monovalent or divalent metals. Addition of 1 mM EDTA resulted in a 96% decrease in activity, consistent with the requirement for divalent metals in the DRE-TIM metallolyase superfamily and suggesting that the enzyme is copurified with a divalent metal. Activity increased 1.5-fold in the presence of 100 mM KCl or NaCl. Addition of 20 mM $MgCl_2$, $MnCl_2$, or $ZnCl_2$ decreased activity.

Under the optimized conditions, MjIPMS exhibits Michaelis−Menten kinetics with respect to both substrates (Figure S2, Supporting Information). A value of 330 ± 5 min^{-1} was determined for k_{cat} at 37 °C, and values of 90 ± 5 and 70 ± 5 μM were determined for K_{KIV} and K_{AcCoA}, respectively. As the DTP-based thiol capture assay reports on only CoA formation, NMR spectroscopy was used to rule out the uncoupled formation of CoA caused by hydrolysis. Using this assay, the formation of acetate could not be detected, which is consistent with the kinetic parameters resulting from the KIV-dependent isopropylmalate formation reaction (Figure S3, Supporting Information). *M. jannaschii* is a hypterthermophilic organism; however, background hydrolysis of AcCoA precluded evaluation of the enzyme at higher temperatures. MjIPMS retains full activity after incubation in water for 15 min at up to 90 °C (Figure S4, Supporting Information). As a control, kinetic parameters were determined at 55 °C. The value for k_{cat} is increased as one would predict (450 ± 30 min^{-1}), but the K_M value for AcCoA is relatively unchanged (95 ± 10 μM).

Effect of pH on Catalytic Parameters. Enzyme assays were performed at various pH values between 5.5 and 9.4 to identify pK_a values for ionizable residues that may be involved in the catalytic mechanism of MjIPMS. Figure 2A shows the effect of pH on k_{cat} values. The data fit best to an equation describing two residues that must be deprotonated (pK_a = 6.3 ± 0.1) and a single residue that must be protonated (pK_a = 8.9 ± 0.1) for full activity. The effect of pH on k_{cat}/K_M values is shown in Figure 2B. In this case, both substrates display bell-shaped profiles with slopes of 2 at the acidic and basic limbs. pK_a values of these residues were similar (6.2 and 6.5 on the acidic limb and 9.1 and 9.2 on the basic limb for varied AcCoA and KIV, respectively).

Primary Deuterium and Solvent Kinetic Isotope Effects. Kinetic isotope effects were used to identify the rate-determining step in the reaction. Primary deuterium effects on the condensation step were determined using [$^2H_3$C]acetyl-CoA (Figure 3). The data were best fit to eq 5, which ascribes the full isotope effect to k_{cat}. A value of 1.3 ± 0.1 was determined for $^{D}k_{cat}$. A $^{D_2O}k_{cat}$ value of 3.1 ± 0.4 is determined by comparing the maximal value for k_{cat} at the pH and pD optima (Figure 2A). The proton inventory technique was used to determine the number of protons in flight that contribute to the solvent kinetic isotope effect (Figure 4). A linear dependence of the $^{D_2O}k_{cat}$ value with respect to the D_2O fraction is consistent with a single proton being responsible for the full solvent kinetic isotope effect. To rule out a contribution from the increase in solvent viscosity in D_2O, a control reaction was conducted in 10% glycerol. The kinetic parameters determined in the presence of glycerol are similar to those determined in water, suggesting solvent viscosity does not contribute to the observed kinetic isotope effect.

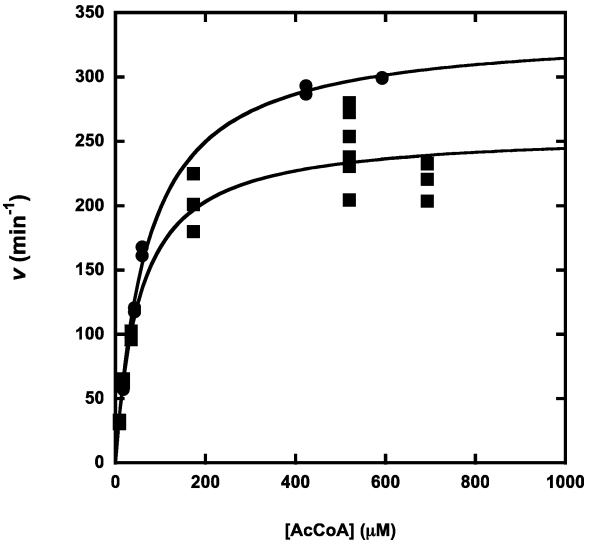

Figure 3. Primary deuterium kinetic isotope effects. Initial velocities using varying amounts of AcCoA (●) and [$^2H_3$C]AcCoA (■) in the presence of saturating concentrations of KIV. Experimental conditions are as described in Materials and Methods. Solid lines are from a fit of the data to eq 5. The following values were determined by the fit: k_{cat} = 336 ± 12 min^{-1}, K_{AcCoA} = 70 ± 7 μM, and $^{D}k_{cat}$ = 1.3 ± 0.1.

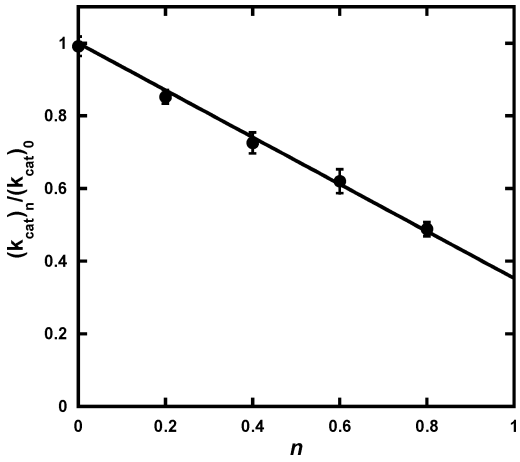

Figure 4. Proton inventory for the MjIPMS solvent kinetic isotope effect. Experimental conditions were as described in Materials and Methods. Error bars represent the standard deviation of results from three independent experiments. The solid line is a fit of the data to eq 7.

Inhibition by L-Leucine. As MjIPMS is predicted to contain the LeuA dimer regulatory domain, it was expected that the enzyme would be inhibited by the addition of L-leucine. Titration of L-leucine into the enzyme assay under k_{cat} conditions indicates it binds tightly to the enzyme with a K_i value of 160 ± 16 nM (Figure 5A). Michaelis−Menten plots determined in the presence of saturating L-leucine concentrations indicate that inhibition is due to a decrease in k_{cat}, while values for the K_M parameters of each substrate are slightly improved (Figure 5B). Results of experiments that aimed to determine a more accurate description of the inhibition mechanism are described below. Consistent with the allosteric

dx.doi.org/10.1021/bi500702u | *Biochemistry* 2014, 53, 4847−4856

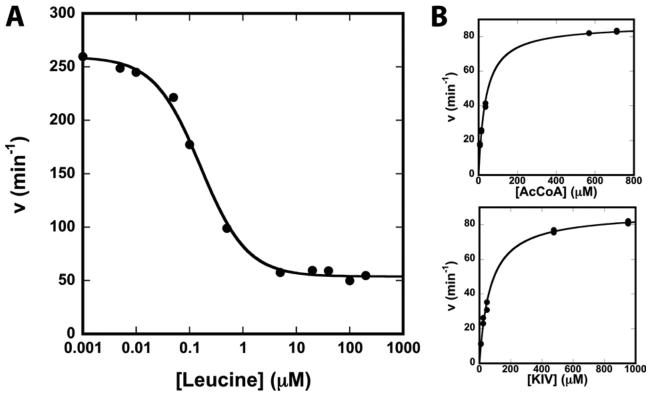

Figure 5. Inhibition of MjIPMS by L-leucine. (A) Titration of varying concentrations of L-leucine on MjIPMS activity in the presence of saturating substrate concentrations. The solid line is a fit of the data to eq 8. (B) Effect of 20 μM L-leucine on the kinetic parameters of MjIPMS. Nonvaried substrates were kept constant at saturating concentrations. Solid lines are fits of initial velocities to eq 1. The following Michaelis constant values were determined: K_{AcCoA} = 36 ± 2 μM, and K_{KIV} = 70 ± 5 μM.

nature of inhibition, MjIPMS retains approximately 20% activity in the presence of saturating L-leucine concentrations.

Effect of L-Leucine on the Quaternary Structure of MjIPMS. Size-exclusion chromatography was used to determine the native molecular weight of MjIPMS (Figure 6). The enzyme eluted from the column as a single peak with a MW_{exp} of 230 kDa, consistent with a tetrameric quaternary structure (MW_{calc} = 226 kDa). The effect of L-leucine on the tetramer was determined by repeating the experiment in the presence of 50 μM L-leucine. In the presence of L-leucine, the enzyme eluted as a single peak with an MW_{exp} of 210 kDa. These results

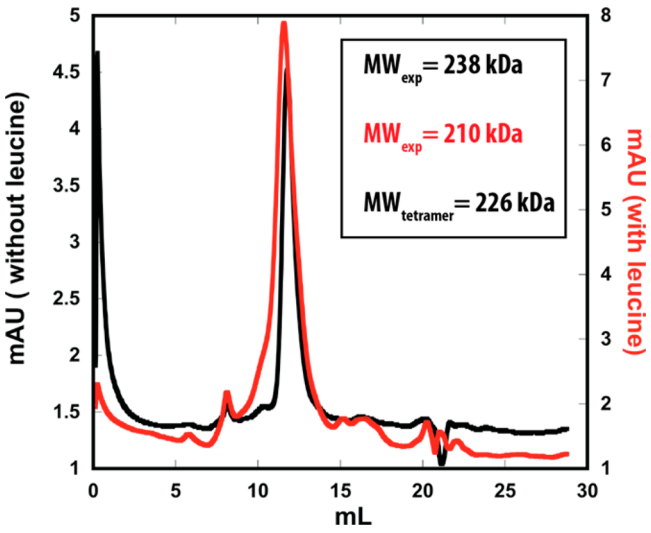

Figure 6. Size-exclusion chromatography results for MjIPMS in the absence and presence of L-leucine. Experimental conditions are as described in Materials and Methods. Protein elution was detected following the absorbance at 280 nm. The black trace shows the elution profile of MjIPMS in the absence of L-leucine and the red trace in the presence of 50 μM L-leucine added to the enzyme and running buffer. Native molecular weights for each peak are calculated as described in Materials and Methods. The predicted molecular weight for the tetramer was calculated by multiplying the calculated monomer weight (56.6 kDa) by 4.

suggest that inhibition of MjIPMS by L-leucine does not rely on changes to the quaternary structure of the enzyme.

Effect of L-Leucine on the Rate-Determining Step. Using the methodology previously described for the characterization of L-leucine inhibition in MtIPMS,[19] kinetic isotope effect experiments were repeated in the presence of L-leucine to determine the target of V-type allosteric inhibition. Primary deuterium isotope effects on $^{D}k_{cat}$ were slightly elevated to 1.6 ± 0.1 in the presence of L-leucine, suggesting there is a small increase in the rate-determining nature of the condensation step (Figure 7A). The $^{D_2O}k_{cat}$ value of 3.1 ± 0.1 was determined

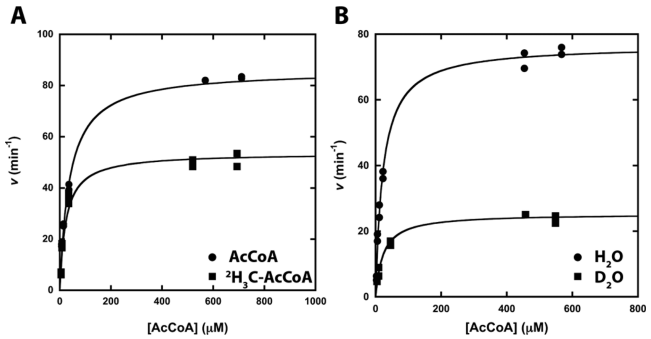

Figure 7. Effect of L-leucine on kinetic isotope effects. (A) Primary kinetic isotope effects in the presence of 20 μM L-leucine. Initial velocities were determined using varying amounts of AcCoA (●) and [^2H_3C]AcCoA (■). Solid lines are from a fit of the data to eq 5. The following values were determined by the fit: k_{cat} = 86 ± 2 min^{-1}, K_{AcCoA} = 38 ± 3 μM, and $^{D}k_{cat}$ = 1.6 ± 0.1. (B) Solvent kinetic isotope effects in the presence of 20 μM L-leucine. Assays were performed in the pL-independent region for k_{cat} (pL 8.2) in H_2O (●) and D_2O (■). Solid lines are from a fit of the data to eq 6. The following values were determined by the fit: k_{cat} = 77 ± 2 min^{-1}, K_{AcCoA} = 23 ± 1 μM, $^{D}k_{cat}$ = 3.0 ± 0.1, and $^{D}k_{cat}/K_M$ = 3.1 ± 0.6.

in the pL-independent region in the presence of L-leucine. This value is similar to that measured in the absence of the inhibitor (3.1 ± 0.4), suggesting the hydrolytic step remains primarily rate-determining in the presence of L-leucine, similar to the mechanism seen with MtIPMS (Figure 7B).

Representative Protein Similarity Network (PSN) for Individual Domains. To look for evidence of co-evolution between the catalytic domain and LeuA dimer regulatory domain of IPMS and CMS enzymes, representative PSNs were constructed from the isolated sequences corresponding to either the DRE-TIM catalytic and linker domains (red and blue ribbon in Figure 1A, MjIPMS 1−368/MtIPMS 1−461) or the LeuA dimer regulatory domain (yellow and orange ribbon in Figure 1A, MjIPMS 369−518/MtIPMS 462−644) (Figure 8). The representative sequence data set was populated using truncated sequences from the previously defined Claisen condensation-like subgroup of the DRE-TIM metallolyase superfamily predicted to contain both catalytic and regulatory domains (cyan nodes in Figure 8A). Overall, 291 representative sequences were collected and subjected to an all versus all BLAST search to define edge values based on *E* value scores. The representative PSNs for the DRE-TIM catalytic/linker domain and LeuA dimer regulatory domain sequences are shown in Figure 8. Edges are drawn if the similarity between two nodes is better than an *E* value cutoff of 10^{-70} for Figure 8A and 10^{-20} for Figure 8B. Cluster membership (IPMS1/CMS1/MAM, IPMS2, CMS2, and CMS3) as defined in Figure 1B was imported as an orthogonal attribute into each new

dx.doi.org/10.1021/bi500702u | *Biochemistry* 2014, 53, 4847−4856

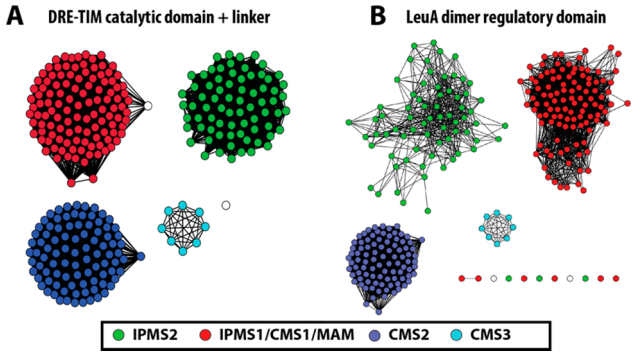

Figure 8. Representative protein similarity network for individual domains of predicted multidomain sequences in the CC-like subgroup. Node coloring is by cluster membership from Figure 1A with IPMS1/CMS1/MAM in red, IPMS2 in green, CMS2 in blue, and CMS3 in cyan. (A) Representative network of sequences corresponding to the catalytic and linker domains from cyan nodes in Figure 1B. Edges are drawn if the similarity between a pair of nodes is better than an *E*-value threshold cutoff of 10^{-70} (median alignment length of 361 residues, median percent identity of pairwise comparisons of 50.5%). (B) Representative network of sequences corresponding to the LeuA dimer regulatory domain from cyan nodes in Figure 1B. Edges are drawn if the similarity between a pair of nodes is better than an *E* value threshold cutoff of 10^{-20} (median alignment length of 155 residues, median percent identity of pairwise comparisons of 41%).

representative network and is represented by different node colors in Figure 8. At these levels of stringency, sequences corresponding to the catalytic/linker and regulatory domains independently separate into clusters identical to those seen when the full-length protein is used to generate the network. If the individual domains had formed unique clusters, each cluster would have multiple colors represented.

DISCUSSION

Chemical Mechanism of MjIPMS. MjIPMS appears to be mechanistically similar to MtIPMS despite the low level of sequence identity (~20%). A multiple-sequence alignment of representative IPMS sequences from both clusters shows that residues predicted to be involved in KIV selectivity (green diamonds, Figure 9) and catalytically essential residues (red circles, Figure 9) are conserved. Analysis of pH−rate profiles shows that MjIPMS, like MtIPMS, uses general acid−base residues in catalysis and both enzymes require a divalent cation for activity. The pH−rate profile for k_{cat} values with MjIPMS shows that pK_a values are shifted approximately 1 unit more acidic than those determined for MtIPMS (Figure 2A). This allows for the characterization of basic residues previously predicted in the mechanism.[21] One of the acidic pK_a values of 6.3 most likely corresponds to the general base used for the initial deprotonation of AcCoA. The second may correspond to the base responsible for deprotonation of water during the hydrolytic step. The identities of these residues are difficult to predict because of the number of conserved, charged residues in the active site and have yet to be experimentally confirmed for IPMS enzymes. The basic pK_a value of 8.9 most likely corresponds to the general acid involved in protonating the α-keto group of KIV upon condensation. A similar basic limb pK_a of 8.0 has been reported for the CC-like subgroup member homocitrate synthase.[28] Structural results from members of the CC-like subgroup indicate the nearest residue capable of playing this role is a conserved arginine (from the DRE motif). This arginine (R32 in MjIPMS and R80 in MtIPMS) is poised to stabilize an enolate intermediate and is essential for activity in MtIPMS.[9] However, a pK_a value of 9 for arginine would require significant perturbation from the active site environment. The source of perturbation is not readily apparent from the available structures. The main catalytic difference noted between MjIPMS and MtIPMS is the rate-determining step in catalysis. Solvent kinetic isotope effects are consistent with hydrolysis as the rate-determining step in catalysis for MjIPMS. This is in contrast to MtIPMS where product release is rate-determining in the absence of L-leucine.[19] However, these are the only two IPMS enzymes to be characterized in this respect, making it difficult to draw a strong correlation to cluster membership.

Allosteric Regulation of MjIPMS. Not surprisingly, L-leucine acts as an inhibitor of activity in MjIPMS similar to other IPMS enzymes. The determined K_i value of 160 nM is approximately 14-fold lower than the overall inhibition constant of 2.3 μM determined for MtIPMS.[17,23] MtIPMS exhibits slow-onset inhibition by L-leucine, while MjIPMS gave linear progress curves in the presence of L-leucine. This suggests either a two-step, slow-onset mechanism does not play a role in MjIPMS inhibition or the binding and conformational change steps occur rapidly. Currently, there is no reported structure for the LeuA dimer regulatory domain from a member of the IPMS1 cluster, making comparisons of residues involved in the regulatory binding site difficult. Interestingly, both enzymes retain significant activity in the presence of saturating inhibitor concentrations. The noncorrelation between the tightness of binding and the degree of inhibition has previously been noted for K-type systems and cited as evidence against a two-state allosteric model.[29] These results suggest similar arguments can be made for V-type systems. Results from size-exclusion chromatography indicate L-leucine does not alter the quaternary structure of the enzyme, consistent with previously characterized IPMS enzymes from both clusters.

Mechanistically, L-leucine acts as a V-type allosteric inhibitor, decreasing the value of k_{cat} while leaving K_M values for the substrates relatively unaffected. Unfortunately, identification of a V-type allosteric mechanism does not provide a significant amount of mechanistic understanding as the affected parameter contains a collection of rate constants that vary depending on the rate-determining step in the catalytic reaction. To address this issue, kinetic isotope effects have been used to identify the rate-determining step in the presence of L-leucine for MjIPMS as previously described for MtIPMS.[19] The solvent kinetic isotope effects are consistent with a rate-determining hydrolytic step in the uninhibited reaction. In the presence of L-leucine, there is a small increase in the primary kinetic isotope effect (from 1.3 to 1.6), but the solvent kinetic isotope effect on k_{cat} remains fully expressed. Thus, two evolutionarily distinct IPMS enzymes with a low level of sequence identity and different quaternary structures appear to utilize identical allosteric mechanisms based on disruption of catalytic machinery involved in the hydrolytic step of the reaction. Currently, it is not clear if the two clusters utilize identical sets of globally conserved residues or differentially conserved residues in members of each cluster. This question is difficult to address, as sequence alignments must include only those enzymes using identical mechanisms of allostery. This highlights the difficulty in identifying structure−function relationships in allosteric mechanisms and emphasizes why caution must be taken when comparing regulatory mechanisms for homologous enzymes.

dx.doi.org/10.1021/bi500702u | *Biochemistry* 2014, 53, 4847−4856

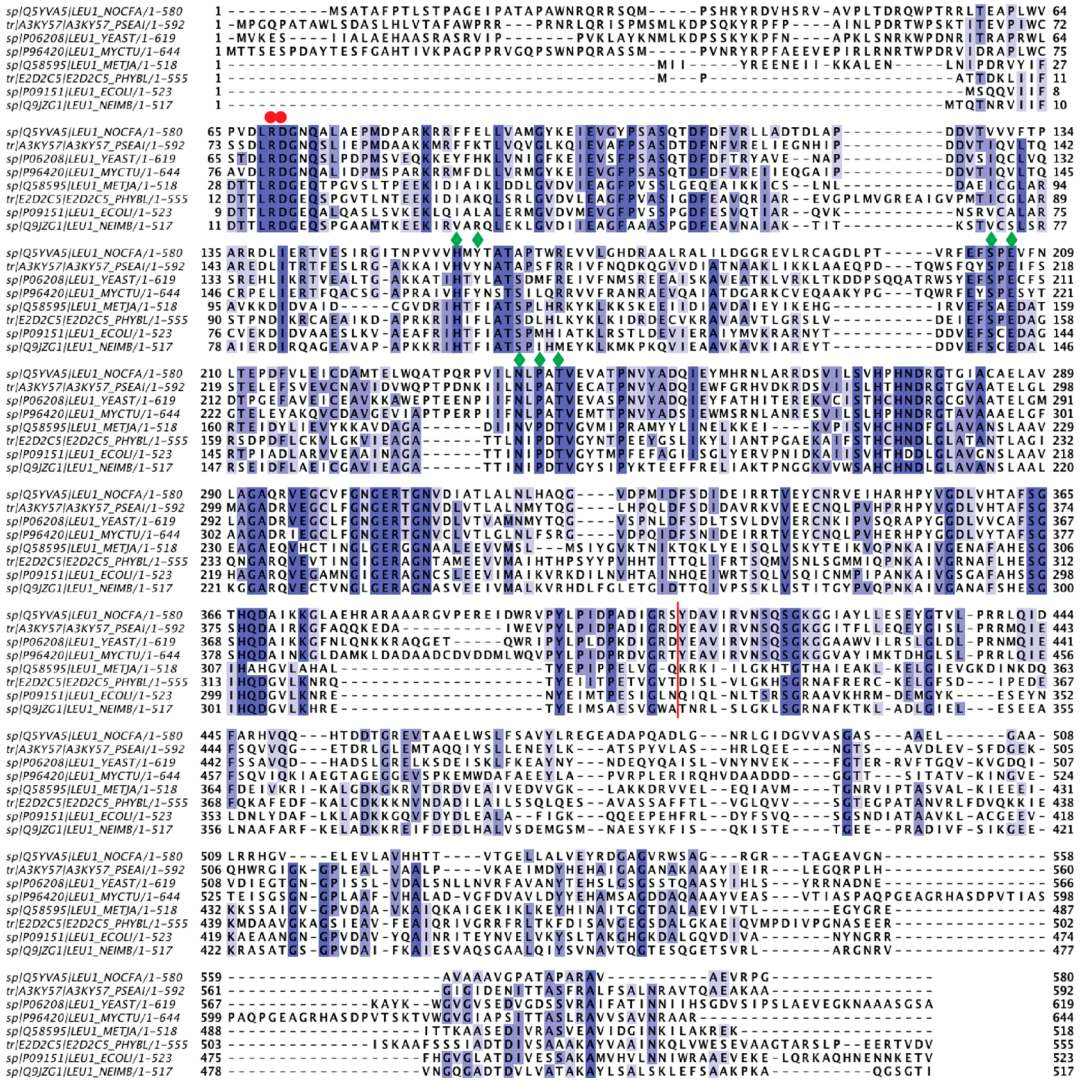

Figure 9. Multiple-sequence alignment of IPMS1 and IPMS2 sequences. A structure-based sequence alignment for the catalytic domains of MtIPMS and IPMS from *Neisseria meningitidis* was created using the Matchmaker alogorithm in Chimera, refined by eye, and used as a seed for the alignment of full-length sequences selected from the IPMS1 (sequences 5−8) and IPMS2 (sequences 1−4) clusters. The multiple-sequence alignment was performed using MAFFT version 7. The red line indicates the end of the structure-based sequence alignment seed. Green diamonds denote residues involved in KIV binding and red circles essential catalytic residues.

Possible Mechanisms for Spurring the Evolution of Multiple Versions of IPMS. An understanding of the evolutionary development of multiple versions of IPMS and the diversity of regulatory mechanisms would be useful in identifying structure−function relationships. Multiple mechanisms have been proposed to explain how enzymes with a low level of sequence identity catalyze the same reactions. A mechanism of divergent evolution, in which different versions evolve from a common progenitor, has been proposed for the appearance of multiple versions of *o*-succinylbenzoate synthase enzymes that use differentially conserved active site residues to accomplish different modes of ligand binding.[13] An alternate mechanism is that of "pseudoconvergent" evolution in which each version evolves from distinct but related progenitors. This mechanism has been proposed to describe the appearance of distinct versions of muconate lactonizing enzyme[15] and *N*-succinyl amino acid racemase.[14] As a result of pseudoconvergent evolution, these enzymes exhibit differences in substrate and stereochemical selectivity. In the absence of phylogenetic data for the DRE-TIM metallolyase superfamily, one cannot rule out either possible mechanism.

From this work, it is clear that in addition to sharing function, enzymes with a low level of sequence identity can share discrete regulatory mechanisms. An explanation for this based on divergent evolution becomes problematic if both the specificity for the substrate and regulatory ligand are to be simultaneously modified. The theory of colocalization has been proposed to address this apparent paradox. Colocalization theory states that interactions between domains or subunits of an enzyme can be forced to evolve through events that increase the local concentration of the two partners, such as gene fusion or compartmentalization.[30] Each colocalization event can create a unique linkage between the two partners, resulting in the evolution of unique structure−function relationships for allosteric mechanisms within a conserved family of enzymes. Thus, a plausible hypothesis for the formation of two distinct IPMS clusters is that the LeuA dimer regulatory domain became fused with two separate, but related, progenitors, resulting in pseudoconvergent evolution.

dx.doi.org/10.1021/bi500702u | *Biochemistry* 2014, 53, 4847−4856

While phylogenetic evidence required to identify the mechanism of evolution used by the CC-like subgroup is lacking, the results of PSNs for the individual domains of the LeuA dimer regulatory domain-containing members indicate significant co-evolution has occurred between the two domains as they individually sort into identical clusters as seen with the full-length enzyme (Figure 8). Previous studies of enzymes containing the LeuA dimer regulatory domain are consistent with this result as removal of the regulatory domain has been shown to affect the functionality of the catalytic domain, including substrate binding in MtIPMS and substrate selectivity in IPMS from *Arabidopsis thaliana*.[31,32] Additionally, allosteric regulation in MtIPMS has been linked to intersubunit communication, in which substitution of residues in the catalytic domain affects inhibitory properties of the regulatory domain.[23] Taken together, these results indicate the importance of integrating catalytic and regulatory mechanisms in multi-domain enzymes.

CONCLUSIONS

This work provides a rigorous catalytic and regulatory description of MjIPMS, an evolutionarily distinct form of IPMS as identified by a protein similarity network of the DRE-TIM metallolyase superfamily. In comparison with MtIPMS, enzymes from the two clusters share similar catalytic properties despite a level of sequence identity of ~20%, with differences occurring in the identity of the rate-determining step. Interestingly, the two enzymes utilize identical mechanisms of allosteric regulation, with both targeting machinery used in the hydrolytic step of the reaction. The identification of distinct enzymes sharing similar allosteric mechanisms despite a low level of sequence identity provides a starting point for the difficult task of identifying structure–function relationships in allosteric mechanisms. Phylogenetic analysis is underway to determine the evolutionary mechanisms responsible for formation of evolutionarily distinct versions of IPMS, but bioinformatics and biochemical studies indicate there is extensive co-evolution of the catalytic and regulatory domains in IPMS enzymes with minimal domain exchange occurring.

ASSOCIATED CONTENT

Supporting Information

Effect of exogenous metal ions on activity, Michaelis–Menten curves for both substrates, NMR spectra of the fully coupled reaction, and thermal stability of MjIPMS. This material is available free of charge via the Internet at http://pubs.acs.org.

AUTHOR INFORMATION

Corresponding Author

*Department of Chemistry, The University of Alabama, Box 870336, Tuscaloosa, AL 35406. E-mail: pfrantom@ua.edu. Telephone: (205) 348-8349. Fax: (205) 348-9104.

Funding

This work was supported by National Science Foundation Grant MCB-1254077 (P.A.F.).

Notes

The authors declare no competing financial interest.

ABBREVIATIONS

AcCoA, acetyl-coenzyme A; CMS, citramalate synthase; CC-like, Claisen condensation-like; DTP, 4,4′-dithiodipyridine; HEPES, *N*-(2-hydroxyethyl)piperazine-*N*′-2-ethanesulfonic acid; HCS, homocitrate synthase; IPTG, isopropyl β-D-1-thiogalactopyranoside; IPMS, α-isopropylmalate synthase; KIV, α-ketoisovalerate; MjIPMS, IPMS from *M. jannaschii*; MtIPMS, IPMS from *My. tuberculosis*; MES, 2-(*N*-morpholino)-ethanesulfonic acid; PSN, protein similarity network; TAPS, *N*-tris(hydroxymethyl)methyl-2-aminopropanesulfonic acid; TEA, triethanolamine.

REFERENCES

(1) Glasner, M. E., Gerlt, J. A., and Babbitt, P. C. (2007) Mechanisms of protein evolution and their application to protein engineering. *Adv. Enzymol. Relat. Areas Mol. Biol. 75*, 193–239 , xii–xiii.

(2) Gerlt, J. A., Babbitt, P. C., Jacobson, M. P., and Almo, S. C. (2012) Divergent evolution in enolase superfamily: Strategies for assigning functions. *J. Biol. Chem. 287*, 29–34.

(3) Gerlt, J. A., and Babbitt, P. C. (2001) Divergent evolution of enzymatic function: Mechanistically diverse superfamilies and functionally distinct suprafamilies. *Annu. Rev. Biochem. 70*, 209–246.

(4) Allen, K. N., and Dunaway-Mariano, D. (2009) Markers of fitness in a successful enzyme superfamily. *Curr. Opin. Struct. Biol. 19*, 658–665.

(5) Glasner, M. E., Gerlt, J. A., and Babbitt, P. C. (2006) Evolution of enzyme superfamilies. *Curr. Opin. Chem. Biol. 10*, 492–497.

(6) Gerlt, J. A., Babbitt, P. C., and Rayment, I. (2005) Divergent evolution in the enolase superfamily: The interplay of mechanism and specificity. *Arch. Biochem. Biophys. 433*, 59–70.

(7) Hicks, M. A., Barber, A. E., II, Giddings, L. A., Caldwell, J., O'Connor, S. E., and Babbitt, P. C. (2011) The evolution of function in strictosidine synthase-like proteins. *Proteins 79*, 3082–3098.

(8) Gerlt, J. A., and Raushel, F. M. (2003) Evolution of function in $(\beta/\alpha)_8$-barrel enzymes. *Curr. Opin. Chem. Biol. 7*, 252–264.

(9) Casey, A. K., Hicks, M. A., Johnson, J. L., Babbitt, P. C., and Frantom, P. A. (2014) Mechanistic and bioinformatic investigation of a conserved active site helix in α-isopropylmalate synthase form *Mycobacterium tuberculosis*, a member of the DRE-TIM metallolyase superfamily. *Biochemistry 53*, 2915–2925.

(10) Koon, N., Squire, C. J., and Baker, E. N. (2004) Crystal structure of LeuA from *Mycobacterium tuberculosis*, a key enzyme in leucine biosynthesis. *Proc. Natl. Acad. Sci. U.S.A. 101*, 8295–8300.

(11) Zhang, P., Ma, J., Zhang, Z., Zha, M., Xu, H., Zhao, G., and Ding, J. (2009) Molecular basis of the inhibitor selectivity and insights into the feedback inhibition mechanism of citramalate synthase from *Leptospira interrogans*. *Biochem. J. 421*, 133–143.

(12) Bulfer, S. L., Scott, E. M., Pillus, L., and Trievel, R. C. (2010) Structural basis for L-lysine feedback inhibition of homocitrate synthase. *J. Biol. Chem. 285*, 10446–10453.

(13) Odokonyero, D., Ragumani, S., Lopez, M. S., Bonanno, J. B., Ozerova, N. D., Woodard, D. R., Machala, B. W., Swaminathan, S., Burley, S. K., Almo, S. C., and Glasner, M. E. (2013) Divergent evolution of ligand binding in the o-succinylbenzoate synthase family. *Biochemistry 52*, 7512–7521.

(14) Song, L., Kalyanaraman, C., Fedorov, A. A., Fedorov, E. V., Glasner, M. E., Brown, S., Imker, H. J., Babbitt, P. C., Almo, S. C., Jacobson, M. P., and Gerlt, J. A. (2007) Prediction and assignment of function for a divergent N-succinyl amino acid racemase. *Nat. Chem. Biol. 3*, 486–491.

(15) Sakai, A., Fedorov, A. A., Fedorov, E. V., Schnoes, A. M., Glasner, M. E., Brown, S., Rutter, M. E., Bain, K., Chang, S., Gheyi, T., Sauder, J. M., Burley, S. K., Babbitt, P. C., Almo, S. C., and Gerlt, J. A. (2009) Evolution of enzymatic activities in the enolase superfamily: Stereochemically distinct mechanisms in two families of cis,cis-muconate lactonizing enzymes. *Biochemistry 48*, 1445–1453.

(16) Frantom, P. A. (2012) Structural and functional characterization of α-isopropylmalate synthase and citramalate synthase, members of the LeuA dimer superfamily. *Arch. Biochem. Biophys. 519*, 202–209.

(17) de Carvalho, L. P., Argyrou, A., and Blanchard, J. S. (2005) Slow-onset feedback inhibition: Inhibition of *Mycobacterium tuber-*

culosis α-isopropylmalate synthase by L-leucine. *J. Am. Chem. Soc. 127*, 10004−10005.
(18) Frantom, P. A., Zhang, H. M., Emmett, M. R., Marshall, A. G., and Blanchard, J. S. (2009) Mapping of the allosteric network in the regulation of α-isopropylmalate synthase from *Mycobacterium tuberculosis* by the feedback inhibitor L-leucine: Solution-phase H/D exchange monitored by FT-ICR mass spectrometry. *Biochemistry 48*, 7457−7464.
(19) Casey, A. K., Schwalm, E. L., Hays, B. N., and Frantom, P. A. (2013) V-type allosteric inhibition is described by a shift in the rate-determining step for α-isopropylmalate synthase from *Mycobacterium tuberculosis*. *Biochemistry 52*, 6737−6739.
(20) Howell, D. M., Xu, H., and White, R. H. (1999) (R)-Citramalate synthase in methanogenic archaea. *J. Bacteriol. 181*, 331−333.
(21) de Carvalho, L. P., and Blanchard, J. S. (2006) Kinetic and chemical mechanism of α-isopropylmalate synthase from *Mycobacterium tuberculosis*. *Biochemistry 45*, 8988−8999.
(22) Quinn, D. M., and Sutton, L. D. (1991) Theoretical Basis and Mechanistic Utility of Solvent Isotope Effects. In *Enzyme Mechanism from Isotope Effects* (Cook, P. F., Ed.) pp 73−126, CRC Press, Boca Raton, FL.
(23) de Carvalho, L. P., Frantom, P. A., Argyrou, A., and Blanchard, J. S. (2009) Kinetic evidence for interdomain communication in the allosteric regulation of α-isopropylmalate synthase from *Mycobacterium tuberculosis*. *Biochemistry 48*, 1996−2004.
(24) Katoh, K., and Standley, D. M. (2013) MAFFT multiple sequence alignment software version 7: Improvements in performance and usability. *Mol. Biol. Evol. 30*, 772−780.
(25) Punta, M., Coggill, P. C., Eberhardt, R. Y., Mistry, J., Tate, J., Boursnell, C., Pang, N., Forslund, K., Ceric, G., Clements, J., Heger, A., Holm, L., Sonnhammer, E. L., Eddy, S. R., Bateman, A., and Finn, R. D. (2012) The Pfam protein families database. *Nucleic Acids Res. 40*, D290−D301.
(26) Altschul, S. F., Madden, T. L., Schaffer, A. A., Zhang, J., Zhang, Z., Miller, W., and Lipman, D. J. (1997) Gapped BLAST and PSI-BLAST: A new generation of protein database search programs. *Nucleic Acids Res. 25*, 3389−3402.
(27) Kohl, M., Wiese, S., and Warscheid, B. (2011) Cytoscape: Software for visualization and analysis of biological networks. *Methods Mol. Biol. 696*, 291−303.
(28) Qian, J., West, A. H., and Cook, P. F. (2006) Acid-base chemical mechanism of homocitrate synthase from *Saccharomyces cerevisiae*. *Biochemistry 45*, 12136−12143.
(29) McGresham, M. S., Lovingshimer, M., and Reinhart, G. D. (2014) Allosteric regulation in phosphofructokinase from the extreme thermophile *Thermus thermophilus*. *Biochemistry 53*, 270−278.
(30) Kuriyan, J., and Eisenberg, D. (2007) The origin of protein interactions and allostery in colocalization. *Nature 450*, 983−990.
(31) Huisman, F. H., Koon, N., Bulloch, E. M., Baker, H. M., Baker, E. N., Squire, C. J., and Parker, E. J. (2012) Removal of the C-terminal regulatory domain of α-isopropylmalate synthase disrupts functional substrate binding. *Biochemistry 51*, 2289−2297.
(32) de Kraker, J. W., and Gershenzon, J. (2011) From amino acid to glucosinolate biosynthesis: Protein sequence changes in the evolution of methylthioalkylmalate synthase in *Arabidopsis*. *Plant Cell 23*, 38−53.